



ORIGINAL ARTICLE

# Effect of three 2-allyl-*p*-mentha-6,8-dien-2-ols on inhibition of mild steel corrosion in 1 M HCl



S. Kharchouf <sup>a</sup>, L. Majidi <sup>a,\*</sup>, M. Bouklah <sup>b</sup>, B. Hammouti <sup>b</sup>,  
A. Bouyanzer <sup>b</sup>, A. Aouniti <sup>b</sup>

<sup>a</sup> *Laboratoire des Substances Naturelles & Synthèse et Dynamique Moléculaire, Faculté des Sciences et Techniques, Université My Ismail, BP 509 Errachidia, Morocco*

<sup>b</sup> *Laboratoire de Chimie Appliquée et Environnement, Faculté des Sciences, Université Mohamed Premier, Oujda, Morocco*

Received 23 October 2010; accepted 3 December 2010

Available online 13 December 2010

## KEYWORDS

Corrosion;  
Inhibition;  
Steel;  
Carvone;  
*p*-Mentha-6,8-dien-2-ol  
derivatives;  
Adsorption

**Abstract** 2-Allyl-*p*-mentha-6,8-dien-2-ols **P1–P3** synthesized from carvone **P** are tested as corrosion inhibitors of steel in 1 M HCl using weight loss measurements, potentiodynamic polarisation and impedance spectroscopy (EIS) methods. The addition of 2-allyl-*p*-mentha-6,8-dien-2-ols reduced the corrosion rate. Potentiodynamic polarisation studies clearly reveal that the presence of inhibitors does not change the mechanism of hydrogen evolution and that they act essentially as cathodic inhibitors. 2-Allyl-*p*-mentha-6,8-dien-2-ols tested adsorb on the steel surface according to Langmuir isotherm. From the adsorption isotherm some thermodynamic data for the adsorption process are calculated and discussed. EIS measurements show the increase of the charge-transfer resistance with the inhibitor concentration. The highest inhibition efficiency (92%) is obtained for **P1** at 3 g/L. The corrosion rate decreases with the rise of temperature. The corresponding activation energies are determined.

© 2011 Production and hosting by Elsevier B.V. on behalf of King Saud University.

## 1. Introduction

The importance of organic compounds on the inhibition of metal corrosion in acid solutions has had much attention during the last decade. The inhibiting action of these compounds is usu-

ally attributed to interactions with metallic surfaces by adsorption. The polar function is frequently regarded as the reaction centre for the adsorption process establishment (Sankarapavinasam et al., 1989), being the adsorption bond strength determined by the electron density and polarizability of the functional group. Recently, we have reported that natural extracts can be a source of cheap eco-friendly and non toxic of inhibitors (Bouyanzer et al., 2006, 2010; Faska et al., 2007, 2008; Ouchikh et al., 2009; Znini et al., 2012).

The widespread occurrence of *p*-menthane system in many classes of natural products has made them a valuable building block for the synthesis of various biologically organic target molecules (Shing et al., 2001; Carter et al., 2000; Meulemans

\* Corresponding author. Tel.: +212 0661422903; fax: +212 0535574485.

E-mail address: lmajidi@yahoo.fr (L. Majidi).

Peer review under responsibility of King Saud University.



Production and hosting by Elsevier

al., 1999; Jennistens et al., 1997). Thus, Synthesis of various *p*-menthane derivatives is extensively studied with the goal to obtain biologically active compounds. *p*-Mentha-6,8-dien-2-one **P** (Carvone) has become the key starting natural compound for the synthesis of a number of substances exhibiting varying kinds of biological activity (Wang et al., 2001). Carvone, a monoterpene ketone, occurs in nature and is widely present in high concentrations in the essential oil of *Mentha specata* (Gershenzon et al., 1989).

In the course of a continuing search for ecofriendly inhibitors of corrosion of steel in acid media, we have studied the effect on the corrosion of steel in 1 M HCl solution of carvone derivatives having various side-chain substituents (2-allyl-*p*-mentha-6,8-dien-2-ols) by gravimetric, potentiodynamic polarisation and impedance spectroscopy (EIS) methods. Effect of temperature is also studied.

## 2. Experimental

### 2.1. Synthesis of 2-allyl-*p*-mentha-6,8-dien-2-ols **P1–P3**

We were the first to accomplish stereoselective synthesis of 2-allyl-*p*-mentha-6,8-dien-2-ols from carvone and allylmagnesium chloride in ether. Condensation of allylmagnesium compounds on carvone leads to 2-allyl-*p*-mentha-6,8-dien-2-ols **P1–P3** in good yields, respectively (Scheme 1). These molecules contain the allylic moiety in the axial position, and the hydroxyl group, in the equatorial position of the cyclohexane ring which adopts a chair conformation (Majidi et al., 2005).

The reaction, in all cases, is stereoselective and the alkylation of **P** takes place on the “*si* face” in a quasi-equatorial fashion. The  $^{13}\text{C}$  NMR spectrum of each alcohol **P1–P3** was consistent with the presence of only one diastereoisomer except for alcohol **P2**. Moreover, we point out that the addition of crotylmagnesium chloride to carvone is not stereoselective. The  $^{13}\text{C}$  NMR spectrum of the corresponding 2-allyl-*p*-mentha-6,8-dien-2-ol **P2** illustrated that this compound existed in the shape of two diastereoisomers (56/44). Thus, only two diastereoisomers have been obtained from the four expected. One deduces that a stereospecific reaction was involved when asymmetric functional carbon has been created. Although, the crotyl magnesium chloride exists almost exclusively in the primary form (Hutchison et al., 1973), it reacts with Carvone such that exclusively  $\alpha$ -methylcarveol products are formed.

The structure of alcohols **P1–P3** was proved by IR and NMR spectroscopy. Their IR spectra lack carbonyl absorption but contain a band at 1650, 3080, and  $3460\text{ cm}^{-1}$ , typical of stretching vibration of C=C bond, the vinylic protons of the

allylic moieties ( $\text{C}=\text{CH}_2$ ) and associated hydroxyl group, respectively. In the  $^1\text{H}$  NMR spectra of these compounds we observed signals from protons of both *p*-menthene fragment and massifs due to protons of allylic moieties (Section 2).

The stereochemistry at the carbinol center of alcohols **P1–P3** was initially assigned based on the relative chemical shifts of the carbinol centers in the  $^{13}\text{C}$  NMR spectra. The signal for the carbinol carbon appears at lower fields for an equatorial than for an axial hydroxyl group (see Section 2) (Stothers et al., 1972). The carbinol signal further downfield should belong to the axial-addition product. These data are consistent with our previous results (Majidi et al., 2004) that the addition of allylic magnesium chloride to cycloalkenone is stereoselective: the attack occurs from the axial side of the molecule.

### 2.2. Synthesis of inhibitors

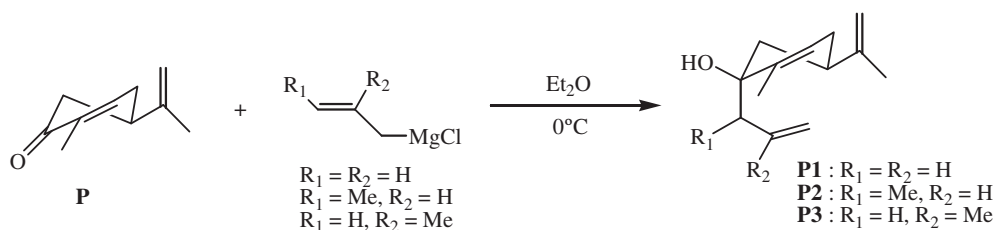
Infrared (IR) spectra were recorded on Schimatzu IR-470.  $^1\text{H}$  NMR spectra were determined on a Brüker AC250 (300 MHz) spectrometer with  $\text{Me}_4\text{Si}$  as the internal standard.  $^{13}\text{C}$  NMR spectra of  $\text{CDCl}_3$  solution were recorded on Brüker AC250 (60 MHz).

#### 2.2.1. General procedure for the addition of allylic Grignard reagents to Carvone: drilling of 2-allyl-*p*-mentha-6,8-dien-2-ols **P1–P3**

Magnesium (1.1 g) was recovered by anhydrous ether (15 ml) and was activated by 1,2-dibromoethane. Upon cessation of gas evolution, the reaction flask was cooled with ice, and a solution of allylic chloride (25 mmol) and menthone (15 mmol) in 70 ml of anhydrous ether was added dropwise. The reaction mixture was stirred in an ice bath for 8 h and then poured onto a diluted sulphuric acid solution. The organic layer was separated and the aqueous layer was extracted with ether. The combined organic layer was washed to neutrality and dried ( $\text{Na}_2\text{SO}_4$ ). The solvent was evaporated and the residual oil was purified by chromatography (silica gel flash, hexane).

#### 2.2.2. 2-Allyl-*p*-mentha-6,8-dien-2-ol ((1*S*,5*R*)-1-(prop-2-en-1-yl)-5-(1-methylvinyl)-2-méthyl- cyclohex-2-énol) **P1**

$\text{C}_{13}\text{H}_{20}\text{O}$ : Rdt = 77%. IR(film): 3400, 3080, 1635,  $1035\text{ cm}^{-1}$ .  $^1\text{H}$  NMR ( $\text{CDCl}_3$ ): 1.50 (2H, t,  $J = 6.4\text{ Hz}$ ), 1.74 (6H, s), 1.92–2.50 (5H, m), 4.73 (2H, s), 5.15 (1H, m), 5.48 (2H, m), 5.88 (1H, m).  $^{13}\text{C}$  NMR ( $\text{CDCl}_3$ ): 17.2 (q), 21.0 (q), 31.0 (t), 39.3 (d), 40.5 (t), 43.0 (t), 73.8 (s), 109.5 (t), 119.1 (t), 124.4 (d), 134.1 (d), 138.2 (s), 149.2 (s).



Scheme 1

### 2.2.3. 2-Allyl-*p*-mentha-6,8-dien-2-ol(1-(1-methylprop-2-en-1-yl)-5-(1-methylvinyl)-2-methyl- cyclohex-2-enol) **P2**

$C_{14}H_{22}O$ : Rdt = 79%. IR(film): 3450, 3080, 1640, 1045  $cm^{-1}$ .  $^1H$  NMR ( $CDCl_3$ ): major isomer (56%): 1.14 (3H, d,  $J = 5.1$  Hz), 1.60 (1H, d,  $J = 5.5$  Hz) 1.76 (6H, s), 2.10 (5H, m), 4.76 (2H, s), 5.02 (1H, m), 5.59 (2H, s), 5.84 (1H, m).  $^{13}C$  NMR ( $CDCl_3$ ): 15.9 (q), 17.9 (q), 21.8 (q), 30.6 (t), 37.2 (t), 38.5 (d), 43.7 (d), 74.9 (s), 110.0 (t), 114.5 (s), 114.7 (t), 125.7 (d), 126.2 (s), 140.3 (d). Minor isomer (44%)  $^1H$  NMR ( $CDCl_3$ ): 0.94 (3H, d,  $J = 5.5$  Hz), 1.74 (6H, s), 4.74 (2H, s), 5.17 (1H, m), 5.65 (2H, s), 6.06 (1H, m).  $^{13}C$  NMR ( $CDCl_3$ ): 15.8 (q), 17.8 (q), 21.6 (q), 31.4 (t), 37.6 (t), 39.4 (d), 44.9 (d), 75.0 (s), 110.1 (t), 116.4 (s), 116.6 (t), 126.2 (s), 126.4 (d), 140.4 (d).

### 2.2.4. 2-Allyl-*p*-mentha-6,8-dien-2-ol((1*S*,5*R*)-1-(2-methylprop-2-en-1-yl)-5-(1-methylvinyl)-2-methylcyclohex-2-enol) **P3**

$C_{14}H_{22}O$ : Rdt = 72%. IR(film): 3450, 3080, 1640, 1043  $cm^{-1}$ .  $^1H$  NMR ( $CDCl_3$ ): 1.61 (2H, s), 1.71 (3H, s), 1.74 (3H, s), 1.84 (3H, s), 2.23 (5H, m), 4.92 (2H, s), 5.43 (2H, s), 5.8 (1H, m).  $^{13}C$  NMR ( $CDCl_3$ ): 17.3 (q), 20.4 (q), 25.0 (q), 31.34 (t), 39.7 (d), 40.7 (t), 46.1 (t), 74.1 (s), 109.4 (t), 115.5 (t), 123.8 (d), 138.8 (d), 142.9 (s), 149.0 (s).

## 2.3. Gravimetric, $R_p$ polarisation and EIS measurements

Steel samples (0.21% C, 0.38% Si, 0.09% P, 0.01% Al, 0.05% Mn, 0.05% S) are used. The aggressive solution (1 M HCl) was prepared by the dilution of analytical grade 37% HCl with bidistilled water. Prior to all measurements, the steel samples were polished with different emery paper up to 1200 grade and washed thoroughly with bidistilled water and dried with acetone.

Gravimetric measurements were carried out in a double walled glass cell equipped with a thermostat-cooling condenser. The solution volume was 100 ml. The steel specimens used had a rectangular form (2 cm  $\times$  2 cm  $\times$  0.05 cm). The immersion time for the weight loss was 1 h at 333 K.

Electrochemical measurements were carried out in conventional three-electrode electrolysis cylindrical Pyrex glass cell. The working electrode (WE) had the form of a disc cut from the steel sheet. The area exposed to the corrosive solution was 1  $cm^2$ . A saturated calomel electrode (SCE) and a disc platinum electrode were used, respectively, as reference and auxiliary electrodes. The temperature was thermostatically controlled at  $298 \pm 1$  K.

Electrochemical experiments were recorded using an EG&G instruments potentiostat-galvanostat model 263A, at scan rate of 0.5 mV/S, coupled to a computer equipped with a software 352 Soft Corr III. Before recording the polarisation curves the test solution was de-aerated and magnetically stirred for 30 min in the cell with pure nitrogen to attain stationary ( $E_{corr}$ ). Gas pebbles was maintained throughout the experiments. WE was then inserted and prepolarised at  $-800$  mV (SCE) for 10 min in order to remove oxide film from the electrode. The scan rate was 1 mV  $s^{-1}$ .

Polarisation resistance measurements were performed by scanning through a potential range which is very close to the corrosion potential. The potential range is  $\pm 10$  mV around  $E_{corr}$ . Polarisation resistance ( $R_p$ ) values are obtained from the current potential plots.

The electrochemical impedance spectroscopy (EIS) measurements were carried out with the electrochemical system (Tacussel) which included a digital potentiostat model Volta-lab PGZ 100 computer at  $E_{corr}$  after immersion in solution without bubbling, the circular surface of steel exposing of 1  $cm^2$  to the solution were used as the working electrode. After the determination of steady-state current at a given potential, sine wave voltage (10 mV) peak to peak, at frequencies between 100 kHz and 10 MHz were superimposed on the rest potential. Computer programs automatically controlled the measurements performed at rest potentials after 30 min of exposure. The impedance diagrams are given in the Nyquist representation.

## 3. Results and discussion

### 3.1. Weight loss tests

The corrosion rate ( $W_{corr}$ ) of steel in 1 M HCl solution at various concentrations of molecule tested was determined after 1 h of immersion period at 333 K. Values of corrosion rates and inhibition efficiencies are given in Table 1. In the case of the weight loss method, the inhibition efficiency ( $E_W\%$ ) was determined by the following relation:

$$E_W(\%) = 100 \times (1 - W_{corr}/W_o) \quad (1)$$

$W_{corr}$  and  $W_o$  are the corrosion rates of steel with and without the inhibitors, respectively.

It has been observed that the inhibition efficiency increased with increasing concentration and reached a maximum value at an optimum concentration 3 g/L. we noted that all compounds used in this study showed very good inhibition of corrosion. The best action is observed with 2-allyl-*p*-mentha-6,8-dien-2-ol **P1** which leads to 92% at 3 g/L.

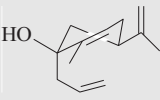
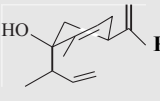

### 3.2. Polarisation measurements

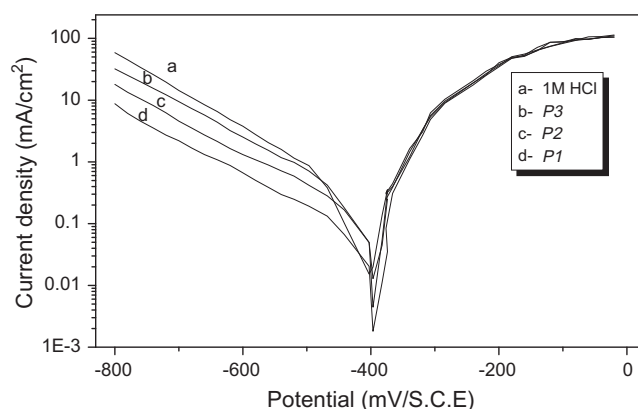
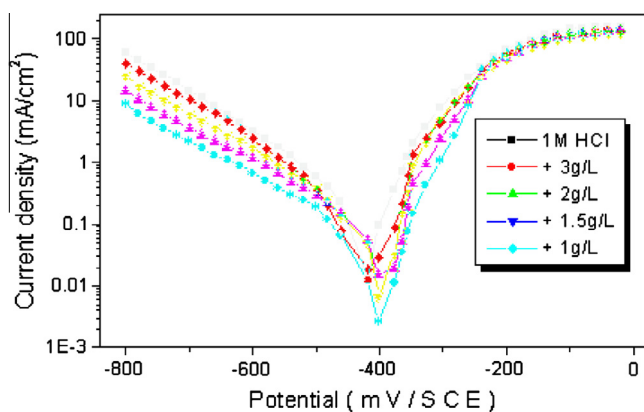
Cathodic and anodic polarisation curves for steel in 1 M HCl in the presence of 3 g/L of **P1**, **P2** and **P3** at 308 K are shown in Fig. 1. In the cathodic domain, it is clear that the current density decreases with the addition of 2-allyl-*p*-mentha-6,8-dien-2-ols compounds; this indicates that these compounds are adsorbed onto the metal surface and hence inhibition occurs.

At the same concentration (3 g/L), the value of  $I_{corr}$  of steel in the case of **P1** is smaller than those of **P2** and **P3**. Compound **P1** gives more inhibition efficiency than **P2** and **P3** in 1 M HCl; this enhanced efficiency is due to the absence of the methyl group in molecule **P1**. The polarisation study confirms the excellent inhibiting character of **P1** obtained with weight loss measurements.

In order to better understand the inhibition mechanism of **P1**, a detailed study on this compound was carried out. Polarisation curves for steel at various concentrations of **P1** in de-aerated normal HCl solutions are shown in Fig. 2. The extrapolation of the Tafel straight line allows the calculation of the corrosion current density ( $I_{corr}$ ). The values of ( $I_{corr}$ ), the corrosion potential ( $E_{corr}$ ), the cathodic Tafel slopes ( $\beta_c$ ) and the corrosion inhibition efficiency ( $E_i\%$ ) for different concentrations of **P1** are given in Table 2. The inhibition efficiency ( $E_i$ ) of the inhibitor for the corrosion of steel was calculated by using corrosion current density as follows:

**Table 1** Influence of 2-allyl-*p*-mentha-6,8-dien-2-ols (**P1–P3**) concentration on the steel corrosion in 1 M HCl at 1 h.

Compounds	C (g/l)	W (mg/cm <sup>2</sup> h)	E (%)
Blank	1 M	12.6776	–
 <b>P1</b>	1	3.5635	71.89
	1.5	2.7688	78.15
	2	2.1579	82.97
	2.5	1.5486	87.78
	3	1.0956	<b>91.38</b>
 <b>P2</b>	1	5.6128	55.72
	1.5	4.6187	63.56
	2	3.7065	70.76
	2.5	3.2589	74.29
	3	2.5138	<b>80.17</b>
 <b>P3</b>	1	6.6625	47.44
	1.5	5.4766	56.8
	2	5.0142	60.44
	2.5	4.4042	65.25
	3	3.5458	<b>72.03</b>

**Figure 1** Polarisation curves of steel in 1 M HCl without and with 3 g/l of **P1**, **P2** and **P3**.**Figure 2** Polarisation curves of steel in 1 M HCl containing various concentrations of **P1**.

$$E_I(\%) = 100 \times (1 - I_{\text{corr}}/I_0) \quad (2)$$

where  $I_0$  and  $I_{\text{corr}}$  are the corrosion current density values without and with the inhibitor, respectively.

It is clear from the results that the addition of inhibitor caused a decrease in the current density. The values of the corrosion current ( $I_{\text{corr}}$ ) of steel in the inhibited solution were smaller than those for the inhibitor free solution. Cathodic current potential curves gave rise to parallel Tafel lines indicating that the hydrogen evolution is activation controlled and the reduction mechanism is not affected by the presence of inhibitors. The addition of inhibitors did not change the values of corrosion potential ( $E_{\text{corr}}$ ) when the concentration increases. These results demonstrated that the hydrogen evolution reaction was inhibited and that the inhibition efficiency increased with inhibitor concentration.

In the anodic range, the polarisation curves of steel in 1 M HCl without and with **P1** show an increase of overvoltage near the corrosion potential. For an overvoltage higher than 240 mV SCE, the presence of inhibitor **P1** does not change the current versus potential characteristics (Fig. 2). This fact means that the inhibition mode of **P1** depends on electrode potential and acts essentially as a cathodic inhibitor. The same results have been reported by other authors (Mengoli et al., 1991). This potential can be defined as the desorption potential. At potential higher than 240 mV SCE, the significant steel dissolution leads to desorption of the inhibiting film. In this case, the desorption rate of **P1** is raised more than its adsorption.

The inhibiting properties of the tested inhibitor have also been evaluated by the determination of the polarisation resistance. The inhibition efficiency ( $E_{R_p}$ ) was defined as follow:

$$E_{R_p}(\%) = 100 \times (1 - R_p/R'_p) \quad (3)$$

$R_p$  and  $R'_p$  are the polarisation resistances in the absence and in the presence of the inhibitor, respectively.

The corresponding polarisation resistance ( $R_p$ ) values of steel in 1 M HCl in the absence of different concentrations of the inhibitor are given in Table 2.

### 3.3. Electrochemical impedance spectroscopy (EIS)

The corrosion behaviour of steel in 1 M hydrochloric acidic solution, in the absence and presence of **P1**, is also

**Table 2** Electrochemical parameters of steel at various concentrations of **P1** studied in 1 M HCl. Corresponding corrosion inhibition efficiencies.

Concentration (g/l)	$E_{\text{corr}}$ (mV/SCE)	$\beta_c$ (mV/dec)	$I_{\text{corr}}$ ( $\mu\text{A}/\text{cm}^2$ )	$E_i$ (%)	$R_p$ ( $\Omega \text{ cm}^2$ )	$E_{R_p}$ (%)
Blank	-396	176	781	–	68	–
1	-400	180	226	71	212	72
1.5	-401	165	190	76	283	76
2	-401	194	156	80	358	81
3	-402	170	100	87	566	88

investigated by the EIS at 308 K after 30 min of immersion. The charge-transfer resistance ( $R_t$ ) values are calculated from the difference in impedance at lower and higher frequencies, as suggested by Tsuru et al. (1978). The double-layer capacitance ( $C_{dl}$ ) and the frequency at which the imaginary component of the impedance is maximal ( $-Z_{\text{max}}$ ) are found as represented in the equation:

$$C_{dl} = 1/\omega \cdot R_t \quad \text{where} \quad \omega = 2\pi f_{\text{max}} \quad (4)$$

where  $f_{\text{max}}$  is the frequency at which the imaginary component of the impedance ( $Z_{\text{im}}$ ) is maximum and  $R_t$  is the diameter of the loop.

Impedance diagrams are obtained for frequency range 100 kHz–10 mHz at the open circuit potential for steel in 1 M HCl in the presence and absence of inhibitor. Nyquist plots for steel in 1 M HCl at 3 g/L of **P1–P3** is presented in Fig. 3. Table 3 gives values of charge-transfer resistance,  $R_t$  double-layer capacitance,  $C_{dl}$ , and  $f_{\text{max}}$  derived from Nyquist plots and inhibition efficiency, the inhibition efficiency got from the charge-transfer resistance is calculated by the following relation:

$$E_{R_t} \% = \frac{R'_t - R_t}{R'_t} \times 100 \quad (5)$$

$R_t$  and  $R'_t$  are the charge-transfer resistance values without and with inhibitor, respectively.

Generally, Fig. 3 showed that the impedance spectra exhibit one single depressed semicircle, and the diameters of semicircle increases with the inhibitors mainly with **P1**. From the results

**Table 3** Impedance parameters of steel in 1 M HCl in the absence and presence of tested compounds at 3 g/L.

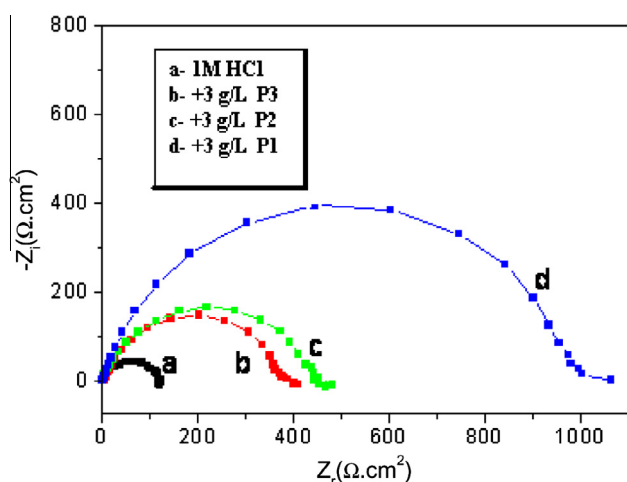
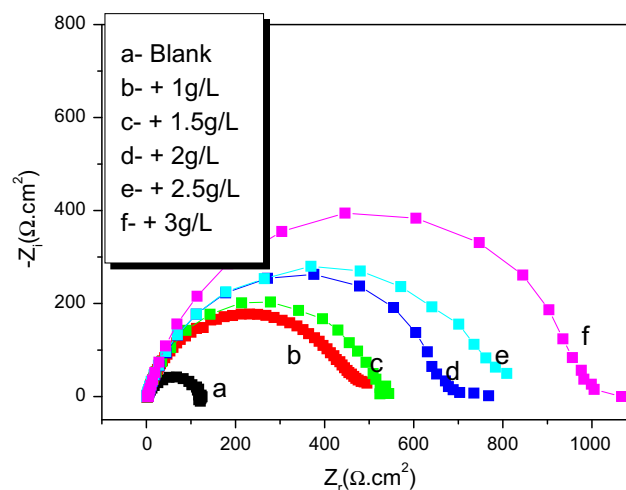
Concentration (M)	$R_t$ ( $\Omega \text{ cm}^2$ )	$F_{\text{max}}$ (Hz)	$C_{dl}$ ( $\mu\text{F}/\text{cm}^2$ )	$E$ (%)
Blank	120	15.86	83.58	–
<b>P3</b>	366	5.53	78.58	67
<b>P2</b>	420	7.33	51.68	71
<b>P1</b>	1000	2.36	67.46	88

of Table 3 and Fig. 4, it is clear that the compound **P1** is the best inhibitor.

In order to better understand the inhibition mechanism of **P1**, a detailed study on this compound was carried out. The impedance parameters are mentioned in Table 3.

In fact, the presence of both inhibitors enhances the value of  $R_t$  in acidic solution. Values of double-layer capacitance are also brought down to the maximum extent in the presence of inhibitor and the decrease in the values of  $C_{dl}$  follows the order similar to that obtained for  $I_{\text{corr}}$  in this study. The decrease in  $C_{dl}$  is due to the adsorption of this compound onto the metal surface leading to the formation of film from acidic solution (Bentiss et al., 1999).

As we notice, the impedance diagrams (Fig. 4) show perfect semi-circles whose size increases with the concentration of the inhibitor indicating a charge-transfer process mainly controlling the corrosion of steel. Similar diagrams were described in the literature for the electrode of iron and steel with and

**Figure 3** Nyquist plots of steel in 1 M HCl containing various compounds at 3 g/L.**Figure 4** Nyquist plots of steel in 1 M HCl at various concentrations of **P1**.

**Table 4** Electrochemical parameters of steel in 1 M HCl + **P1** at various concentrations and the corresponding inhibition efficiency.

Concentration (M)	$R_t$ ( $\Omega \text{ cm}^2$ )	$F_{\max}$ (Hz)	$C_{dl}$ ( $\mu\text{F}/\text{cm}^2$ )	$E$ (%)
Blank	120	15.86	83.58	–
1 g/L	480	4.18	79.32	75
1.5 g/L	522	3.95	77.15	77
2 g/L	667	3.25	73.45	82
2.5 g/L	800	2.82	70.65	85
3 g/L	1000	2.36	67.46	88

without inhibitor 1 M HCl (Elachouri et al., 2001; Bentiss et al., 1999). From the impedance data, the charge-transfer resistance ( $R_t$ ) increases with the inhibitor concentration (Table 4). Also, the double-layer capacitance ( $C_{dl}$ ) decreases with increase in the concentration of the inhibitor.

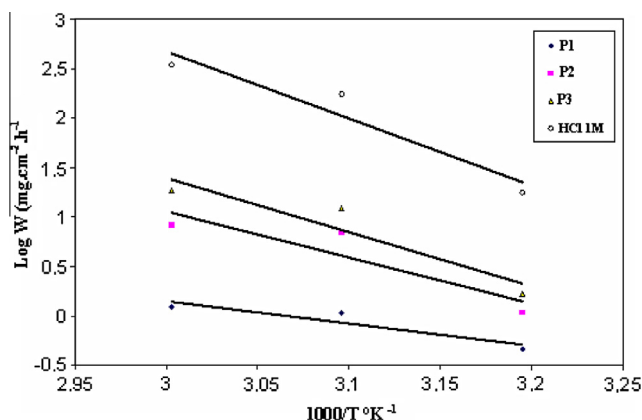
### 3.4. Effect of temperature

The corrosion rate of steel with temperature was studied in molar HCl both in the absence and presence of inhibitor at a maximal concentration (3 g/L) in the temperature range 313–343 K using weight loss measurements, the corresponding results are summarised in Table 5. The corrosion rate is more increased with the rise of temperature for uninhibited acid solution. The presence of inhibitor leads to a decrease in the corrosion rate. The inhibitory action of inhibitor is slightly increased at elevated temperature leading to the increase of  $E\%$ . The apparent activation energy is easily determined by the following relations:

$$W_{\text{corr}} = k \exp(-E_a/RT) \text{ and } W'_{\text{corr}} = k' \exp(-E'_a/RT) \quad (6)$$

$W'$  and  $W^\circ$  are the corrosion rates of steel with and without inhibitor, respectively.  $E'_a$  and  $E_a$  are the apparent activation energies in the presence and absence of inhibitor, respectively.

Straight lines of Arrhenius slopes are obtained. The evaluation of activation energies is deduced from the corresponding slopes (Fig. 5). Values obtained are 50.90, 18.52, 38.50 and 45.27 kJ/mol for free acid and in added with **P1**, **P2** and **P3**, respectively. It is obviously seen that the activation energy strongly decreases in the presence of inhibitors. Some authors (Donahue et al., 1965; Banejee et al., 1992), attributed this

**Figure 5** Arrhenius plots for steel in 1 M HCl in the absence and presence of **5**, **6** and **7**.

result to that the inhibitor species are physically adsorbed onto the metal surface.

### 3.5. Adsorption isotherm

The values of surface coverage  $\theta$  for different concentrations of the inhibition in acidic media of different compounds were evaluated from weight loss using the equation (Landolt et al., 1993):

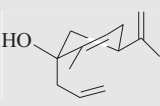
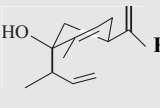
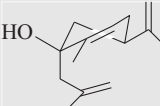
$$\theta = \frac{W_{(\theta=0)} - W_\theta}{W_{(\theta=0)} - W_{(\theta=1)}} \quad (7)$$

The surface coverage values  $\theta$  were tested graphically for fitting a suitable adsorption isotherm. The plot of  $C_{\text{inh}}/\theta$  versus  $C_{\text{inh}}$  yields a straight line, proving that the adsorption of the inhibitors from HCl solution on the steel surface. This shows that Langmuir isotherm (Langmuir, 1947) is accurate in all cases (Fig. 6):

$$\frac{C_{\text{inh}}}{\theta} = \frac{1}{b} + C_{\text{inh}} \quad (8)$$

$$b = \frac{1}{55.5} \cdot \exp\left(-\frac{\Delta G^\circ_{\text{ads}}}{R \cdot T}\right) \quad (9)$$

**Table 5** Effect of temperature (313–343 K) on the corrosion inhibition of steel 1 M HCl by 2-allyl-*p*-mentha-6,8-dien-2-ols (**P1**–**P3**) at 1 h.

Compounds	$T$ ( $^\circ\text{C}$ )	$W$ ( $\text{mg}/\text{cm}^2\text{h}$ )	$W_0$ ( $\text{mg}/\text{cm}^2\text{h}$ )	$E$ (%)
 <b>P1</b>	313	0.71386	3.4780	79.47
	323	1.0312	9.41863	89.04
	333	1.0965	12.6776	91.35
	343	2.0277	19.369	89.5
 <b>P2</b>	313	1.0367	3.4780	70.19
	323	2.324	9.41863	75.3
	333	2.5138	12.6776	80.17
	343	6.4713	19.369	66.58
 <b>P3</b>	313	1.2503	3.4780	64.04
	323	2.9630	9.41863	68.54
	333	3.5458	12.6776	72.03
	343	7.1960	19.369	62.84



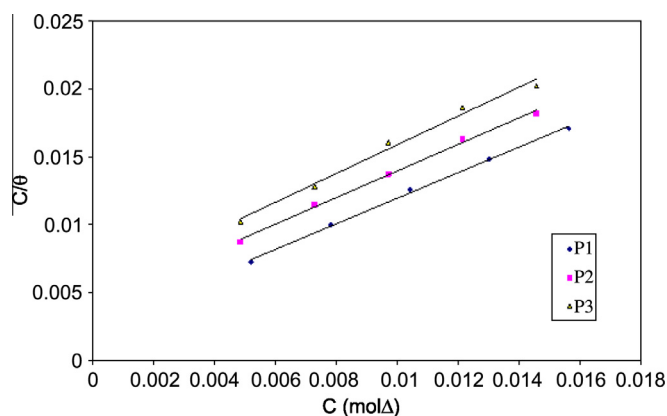


**Figure 6** Langmuir isotherm adsorption model of inhibitors on the surface of steel in 1 M HCl.

$C_{inh}$  is the inhibitor concentration;  $\theta$  is the fraction of the surface covered,  $b$  is the adsorption coefficient and  $\Delta G_{ads}^{\circ}$  is the standard free energy of adsorption.

The  $\Delta G_{ads}^{\circ}$  were estimated from the equilibrium constant  $b$  deduced from the intercept of linear plots:  $\Delta G_{ads}^{\circ}(\mathbf{P1}) = -25.0 \text{ kJ/mol}$ ,  $\Delta G_{ads}^{\circ}(\mathbf{P2}) = -23.7 \text{ kJ/mol}$ ,  $\Delta G_{ads}^{\circ}(\mathbf{P3}) = -23.1 \text{ kJ/mol}$ .

Analysis of results shows that the inhibitor **P1**, which gives maximum efficiency exhibits more negative of  $\Delta G_{ads}^{\circ}$  indicating that it is strongly adsorbed on the metal surface. In general, the negative values of  $\Delta G_{ads}^{\circ}$  indicate the spontaneous adsorption of inhibitors on the steel surface (Talati et al., 1983). A value of  $-40 \text{ kJ/mol}$  for  $\Delta G_{ads}^{\circ}$  is usually adopted as a threshold value between chemisorption and physisorption (Donahue et al., 1965) then, this value indicates that inhibitor interacts on the steel surface by electrostatic effect.

#### 4. Conclusion

From the overall experimental results the following conclusions can be deduced:

1. 2-Allyl-*p*-mentha-6,8-dien-2-ols compounds **P1–P3** act as good inhibitors for the corrosion of steel in HCl medium.
2. The inhibition efficiency increases with the 2-allyl-*p*-mentha-6,8-dien-2-ols concentration to attain 92% at 3 g/l for **P1**.
3. The inhibition efficiency of 2-allyl-*p*-mentha-6,8-dien-2-ols increases with the rise of temperature.

#### References

Banejee, G., Malhotra, S.N., 1992. Corrosion 48, 10.  
 Bentiss, F., Lagrene, M., Traisnel, M., Hornez, J.C., 1999. Corros. Sci. 41, 789.  
 Bouyanzer, A., Hammouti, B., Majidi, L., 2006. Mater. Lett. 60, 2840.

Bouyanzer, A., Hammouti, B., Majidi, L., 2010. Port. Elect. Acta 28, 165.  
 Carter, R., Hodgetts, K., McKenna, J., Magnus, P., Wren, W., 2000. Tetrahedron 56, 4367.  
 Donahue, F.M., Nobe, K., 1965. J. Electrochem. Soc. 112, 886.  
 Elachouri, M., Infante, M.R., Izquierdo, F., Kertit, S., Gouttaya, H.M., Nciri, B., 2001. Corros. Sci. 43, 19.  
 Faska, Z., Majidi, L., Fihi, R., Bouyanzer, A., Hammouti, B., 2007. Pigm. Res. Techn. 36, 293.  
 Faska, Z., Bellioua, A., Bouklah, M., Majidi, L., Fihi, R., Bouyanzer, A., Hammouti, B., 2008. Monatsh. Chem. 139, 1417.  
 Gershenzon, J., Maffei, M., Croteau, R., 1989. Plant Physiol. 89, 1351.  
 Hutchison, D.A., Beck, K.R., Benkeser, R.A., Grutzner, J.B., 1973. J. Am. Chem. Soc. 95, 705.  
 Jenniskens, H.D.L., de Groot, A., 1997. Tetrahedron Lett. 38, 7463.  
 Landolt, D., 1993. Corrosion et Chimie de Surface des Métaux, first ed. Alden Press, Oxford, p. 495.  
 Langmuir, I., 1947. J. Am. Chem. Soc. 69, 1848.  
 Majidi, L., Fihi, R., 2004. Phys. Chem. News 9, 92.  
 Majidi, L., Fihi, R., El Idrissi, M., Kharchouf, S., 2005. Phys. Chem. News 25, 127.  
 Mengoli, G., Musiani, M.M., Pugara, C., Paolucci, F., 1991. Corros. Sci. 32, 743.  
 Meulemans, T.M., Stork, G., Macaev, A., Jansenm, F.Z., de Groot, A., 1999. J. Org. Chem. 64, 9178.  
 Ouachikh, O., Bouyanzer, A., Bouklah, M., Desjobert, J.-M., Costa, J., Hammouti, B., Majidi, L., 2009. Surf. Rev. Lett. 16, 49.  
 Sankarapavinasam, S., Pushpanaden, F., Ahmed, M.F., 1989. Bull. Electrochem. 5, 319.  
 Shing, T.K.M., Lee, C.M., Lo, H.Y., 2001. Tetrahedron Lett. 42, 8361.  
 Stothers, J.B., 1972. Carbon 13 NMR spectroscopy. Academic Press, New York, NY.  
 Talati, J.D., Gandhi, D.K., 1983. Corros. Sci. 23, 1315.  
 Tsuru, T., Haruyama, S., Gijutsu, B., 1978. J. Jpn. Soc. Corros. Eng. 27, 573.  
 Wang, J., Froeyen, M., Hendrix, C., Andrei, C., Snoeck, R., Lescrinier, E., De Clerq, E., Herdewijn, P., 2001. Nucleos. Nucleot. Nucl. Acids 20, 727.  
 Znini, M., Majidi, L., Bouyanzer, A., Paolini, J., Desjobert, J.-M., 2012. Arabian Journal Chem. 5 (4) 467.